Triple Resonant Four-Wave Mixing Boosts the Yield of Continuous Coherent Vacuum Ultraviolet Generation

Daniel Kolbe,* Martin Scheid,† and Jochen Walz

Institut für Physik, Johannes Gutenberg-Universität Mainz and Helmholtz-Institut Mainz, D-55099 Mainz, Germany

(Received 2 April 2012; published 7 August 2012)

Efficient continuous-wave four-wave mixing by using three different fundamental wavelengths with individual detunings to resonances of the nonlinear medium is shown. Up to 6 μW of vacuum ultraviolet light at 121 nm can be generated, which corresponds to an increase of three orders of magnitude in efficiency. This opens the field of quantum information processing by Rydberg entanglement of trapped ions.

DOI: 10.1103/PhysRevLett.109.063901 PACS numbers: 42.65.−k, 32.80.Ee, 32.80.Qk

Continuous-wave coherent radiation in the vacuum ultraviolet (VUV) wavelength region at 121 nm will be essential for future laser-cooling of trapped antihydrogen [1]. Cold antihydrogen will enable both tests of the fundamental symmetry between matter and antimatter at unprecedented experimental precision [2] and also experiments in antimatter gravity [3]. Another fascinating application of narrow band continuous laser radiation in the VUV is quantum information processing using single trapped ions in Rydberg-states [4,5]. There the powerful tool of entanglement by the Rydberg blockade mechanism is used to generate fast qubit operations without involving vibrational modes of the ionic chain.

VUV laser radiation can be generated by four-wave sum-frequency mixing (FWM) in gases and metal vapors [6–8], a process in which three laser fields generate a nonlinear polarization which acts as the driving term for the fourth coherent field at the sum-frequency. A two-photon resonance is known to dramatically enhance the FWM efficiency [9]. To further increase the efficiency the use of one-photon resonances is desirable. However, the dispersion of close one-photon resonances affects phase matching between the driving nonlinear polarization and the generated field in the VUV which can severely limit the efficiency of the FWM process. In this Letter, we show that the interplay of two resonances at one- and three-photon height can be used to cancel phase matching limitations and to take full benefit of the enhancement in the nonlinear susceptibility. Powers of up to 6 μW at 121.26 nm wavelength were achieved. This is 30 times more power than previously reported [10–12] and three orders of magnitude more efficient.

Our experiment uses mercury vapor as a nonlinear medium and the relevant energy levels are shown in Fig. 1(a). A UV beam at 254 nm and a blue beam at 408 nm wavelength are tuned to the two-photon resonance between the 6^1S ground state and the 7^1S state. The third beam at 540 nm can be tuned such that the sum frequency of the three fundamental beams is near the 6^1S–12^1P resonance, which is at 121.26 nm wavelength.

A schematic of the laser system to produce the three fundamental beams is shown in Fig. 1(b). The beam at 254 nm is produced by a frequency-quadrupled Yb:YAG disc laser (ELS, VersaDisk 1030-50). Frequency-quadrupling is done with two resonant enhancement cavities, the first one using a lithium triborate crystal (LBO) as nonlinear medium, the second one using a β-barium borate crystal. From 2 W of infrared light at 1015 nm we get up to 200 mW of UV radiation. This system is capable of producing up to 750 mW of UV light, for details see Ref. [13]. The second fundamental beam at 408 nm is produced by a frequency-doubled titanium:sapphire laser (Coherent, 899-21), pumped by a frequency doubled Nd : YVO_4 laser (Coherent, V10). The external frequency-doubling cavity uses a LBO crystal. From 1.5 W of infrared light at 816 nm, we get up to 500 mW of blue light. The third fundamental beam at 540 nm is produced with a grating stabilized diode laser at 1080 nm boosted by a fiber amplifier system (Koheras, Boostik) and frequency doubled by a modified commercial frequency-doubling cavity (Spectra Physics, Wavetrain). This system is capable of producing up to 4 W of green light at 545.5 nm [14]. For the present experiments, we operate the fiber amplifier at an output power of 740 mW, which gives 280 mW of green light at 540 nm. The beams are overlapped at dichroitic mirrors and focused in the vacuum chamber which contains the mercury vapor. The four-wave mixing region is separated from the detection region by a vacuum sealed MgF_2 lens, which also performs the wavelength separation of the VUV light from the fundamental beams [see Fig. 1(b)]. Due to the dispersion of this lens, the focal length differs for the VUV wavelength ($f = 21.5$ cm at 540 nm, $f = 13$ cm at 121 nm). A tiny mirror is placed in the focus of the fundamental beams to reflect them to the side. The VUV beam is large at the fundamental focus ($w \approx 4.9$ mm) and therefore, the mirror just casts a shadow in the VUV beam, causing $\approx 30\%$ loss. A solar-blind photomultiplier tube is used for detection of the VUV photons. The background is suppressed by four 121 nm transmission filters. The overall detection efficiency due to losses in the MgF_2 lens, the tiny

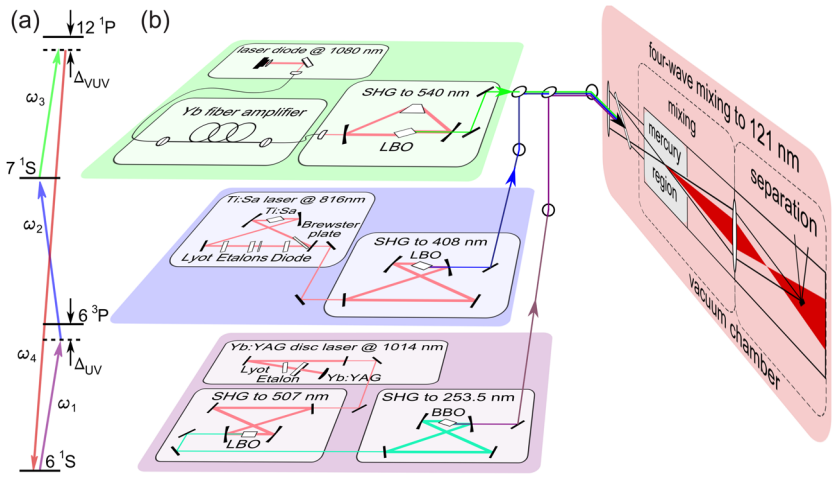

FIG. 1 (color online). (a) Energy-level diagram of mercury. The UV laser (254 nm) is tuned close to the 6^1S–6^3P resonance and the blue laser beam (408 nm) establishes the two photon resonance with the 7^1S state. The green laser is at 540 nm, so that the resulting wavelength is close to the 6^1S–6^3P resonance. (b) Four-wave mixing scheme and setup. The fundamental beams at 254, 408, and 540 nm wavelength are produced by frequency-doubling and frequency-quadrupling of strong continuous-wave solid-state infrared lasers. The beams are shaped, overlapped and focused into the mercury cell where VUV generation takes place. The VUV beam is separated from the fundamental beams by the dispersion of a MgF_2 lens and four VUV filters. A solar-blind photomultiplier tube (not shown) is used for detection (SHG: second harmonic generation, LBO: lithium triborate crystal, BBO: β-barium borate crystal).

mirror, the four filters, and the photomultiplier efficiency is 9×10^{-7}.

The power at the sum frequency $\omega_4 = \omega_1 + \omega_2 + \omega_3$ is given by Bjorklund [15]:

$$P_4 = \frac{9}{4}\frac{\omega_1\omega_2\omega_3\omega_4}{\pi^2\epsilon_0^2c^6}\frac{1}{b^2}\left(\frac{1}{\Delta k_a}\right)^2|\chi_a^{(3)}|^2P_1P_2P_3G(bN\Delta k_a). \tag{1}$$

Here, ω_i is the angular frequency, P_i the power of the ith beam, N the density of the nonlinear medium, $\chi_a^{(3)}$ the nonlinear susceptibility per atom, and $\Delta k_a = (k_4 - k_1 - k_2 - k_3)/N$ the wave vector mismatch per atom. $G(bN\Delta k_a) = \pi^2(bN\Delta k_a)^4\exp(bN\Delta k_a)$ (for $bN\Delta k_a < 0$) is the phase matching function for phase matching by the density of the nonlinear medium with a maximum value at $bN\Delta k_a = -4$ [15]. Equation (1) describes a four-wave mixing process in a nonabsorbing gaseous medium of tightly focused fundamental beams with equal confocal parameters b.

Two important factors are the nonlinear susceptibility $\chi_a^{(3)}$ and the wave vector mismatch Δk_a, which are both independent of the density but functions of the fundamental and sum frequencies. The leading term in the nonlinear susceptibility per atom is given by Smith and Alford [16]:

$$\chi_a^{(3)} = \frac{1}{6\epsilon_0\hbar^3}\sum_{m,n,v}\frac{1}{\omega_{ng} - (\omega_1 + \omega_2)}\frac{\rho_{nm}\rho_{mg}}{\omega_{gm} - \omega_1}\frac{\rho_{nv}\rho_{vg}}{\omega_{gv} - \omega_4}. \tag{2}$$

Here, ω_{ij} is the transition frequency from the initial state i to the final state j and ρ_{ij} is the corresponding dipole matrix moment. The states m and v are linked to the ground state g via a dipole transition at ω_1 and ω_4, respectively. State n is connected to the ground state via a two-photon transition. In the case of FWM with a two-photon resonance and near one-photon resonances for both one fundamental and the generated beam, most of the terms in the sum are negligible and the nonlinear susceptibility is proportional to products of terms related to both resonances. Divergencies at resonances are damped by radiative decay etc., which corresponds to the linewidths. This is not shown in Eq. (2) but taken into account in the calculations. The strong enhancement of the nonlinear susceptibility $\chi_a^{(3)}$ near the 6^1S–12^1P resonance is illustrated in Fig. 2(a).

The wave vector mismatch Δk_a is dominated by the UV and VUV beam. To see this, we write the individual wave vectors k_i, $i = 1 \ldots 4$ as $k_i/N = \omega_i\Re\sqrt{1 + \chi^{(1)}(\omega_i)}$. The square-root term is the refractive index and $\Re$ denotes the real part. $\chi^{(1)}(\omega_i)$ is the linear susceptibility per atom which can be written as

$$\chi^{(1)}(\omega_i) = \frac{2N}{3\epsilon_0\hbar}\sum_v\frac{\omega_{gv}\rho_{gv}^2}{\omega_{gv}^2 - \omega_i^2}, \tag{3}$$

where v represents all the states which connect to the ground state g via a dipole transition. Clearly, resonant terms dominate $\chi^{(1)}$. Expanding the square-root terms in k_i/N, we can, thus, neglect the nonresonant $\chi^{(1)}$ contributions of the blue and green beams and obtain

$$\Delta k_a \approx \frac{1}{3c\epsilon_0\hbar}\sum_v\omega_{gv}\rho_{gv}^2\left(\frac{\omega_4}{\omega_{gv}^2 - \omega_4^2} - \frac{\omega_1}{\omega_{gv}^2 - \omega_1^2}\right). \tag{4}$$

When both frequencies are red-detuned to resonances both terms are positive. To achieve a negative Δk_a (which is

necessary for phase matching), the second term, which is due to the resonance of the fundamental beam, has to be larger than the first term, which is due to the resonance of the generated FWM beam. In Fig. 2(b), the wave vector mismatch Δk_a is shown as a function of the VUV detuning (red solid curve). Near the one-photon resonance, it changes sign and phase matching can not be achieved by adjusting the density of the nonlinear medium. This can be also seen by the divergence of the phase matching density [green dashed line in Fig. 2(b)] at the zero crossing of Δk_a.

The power at the FWM frequency is proportional to $(|\chi_a^{(3)}|/\Delta k_a)^2$ when the phase matching function $G(Nb\Delta k_a)$ is maximized and is shown in Fig. 2(c). The red solid line represents the power at perfect phase matching. Here, the density has to be adjusted as shown in Fig. 2(b). However, in the experiment a too strong increase of the mercury density is not useful because of absorption. For the green dashed line, we took this into account and fixed the density at the phase matching density, in the case of FWM, far from the one-photon resonance ($N = 1 \times 10^{23}$ m^{-3}). The strong increase in the FWM efficiency is due to the combination of two single one-photon resonances: one (UV) to dominate the phase matching and one (VUV) to take full benefit of the increase in the nonlinear susceptibility.

Experimentally, there are three free parameters for the FWM process: the detuning of the UV beam to the 6^1S–6^3P transition (Δ_{UV}), the detuning of the VUV beam to the 6^1S–12^1P transition (Δ_{VUV}), and the density of the mercury vapor (N), which can be adjusted by changing the temperature of the mercury cell. The density affects both the phase matching of the FWM process and the absorption of the VUV beam. The detunings affect the nonlinear susceptibility and the wave vector mismatch and thus, also the phase matching. The optimal density for FWM at a specific set of detunings results from a combination of nearly perfect phase matching and small absorption. To separate these two effects, we have varied the position of the focus in the mercury vapor. This changes the path length of the VUV beam in the mercury vapor region and thus, the absorption length. The absorption coefficient at the VUV wavelength is obtained from the exponential decrease in the FWM efficiency.

The nonlinear susceptibility takes full benefit of smaller detunings at the VUV wavelength, if the dispersion at the VUV wavelength does not adversely effect the phase matching; i.e., the wave vector mismatch in Eq. (4) is still negative because of the dispersion at the UV wavelength (second term). Smaller UV detunings enable a larger FWM efficiency due to the possibility to choose smaller VUV detunings since they contribute with opposite signs to the wave vector mismatch. This is observed in the experiment and shown in Fig. 3. At every UV detuning, the FWM efficiency gains by choosing smaller VUV detunings. The maximum in the FWM efficiency depends on the UV detuning and changes from $\Delta_{\mathrm{VUV}} = 60$ GHz at $\Delta_{\mathrm{UV}} = 400$ GHz to $\Delta_{\mathrm{VUV}} = 30$ GHz at $\Delta_{\mathrm{UV}} = 120$ GHz. At detunings smaller than the optimum, the VUV yield decreases for two reasons:

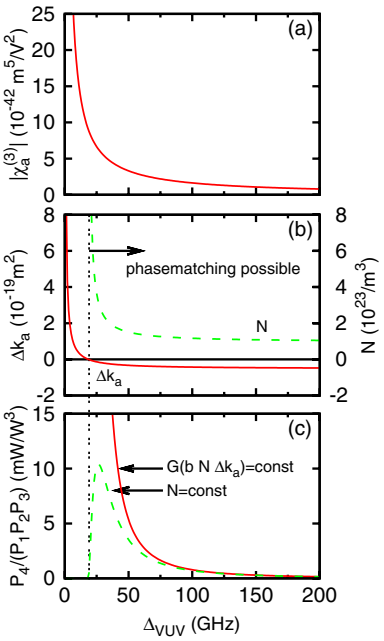

FIG. 2 (color online). Calculation of the FWM power. (a) nonlinear susceptibility, (b) wave vector mismatch (red solid) and phase matching density (green dashed), (c) FWM efficiency at perfect phase matching (red solid) and constant density (green dashed) versus the detuning of the FWM frequency. The UV detuning to the 6^3P level is 200 GHz.

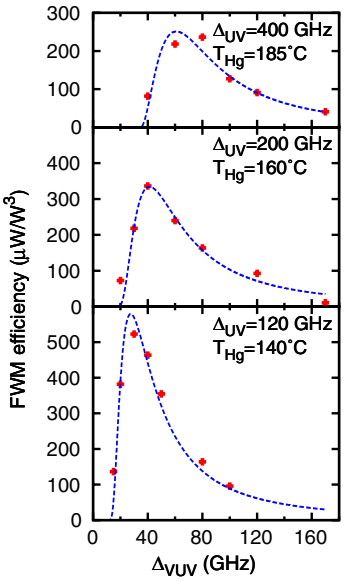

FIG. 3 (color online). FWM efficiency as a function of the detuning to the 12^1P state at different UV detunings to the 6^3P state. The dashed lines are calculations which include imperfect beam overlap of the fundamental beams, absorption at the VUV frequency, and saturation.

absorption of the VUV beam due to the near resonance and a change in the phase matching.

The dashed lines in Fig. 3 are calculations of the FWM efficiency which include absorption at the VUV and UV wavelength. For every combination of detunings, the nonlinear susceptibility per atom $\chi_a^{(3)}$ and the wave vector mismatch per atom Δk_a are calculated. The FWM equation (1) does not include absorption. Absorption of the fundamental beams is taken into account by using the fundamental powers at the position of the focus and thus, at the FWM region. Absorption of the VUV beam is included by an exponential decay from the focus on over the length of the mercury cell. The influence of absorption on the FWM phase matching can be neglected if absorption within the Rayleigh region of the fundamental beams is small. At a UV detuning of 50 GHz and a density of $3.8 \times 10^{22}/\mathrm{m}^{-3}$, we get about 3% of absorption within the Rayleigh length of 0.8 mm.

Let us now compare the absolute value of the observed efficiency in the experiment at a UV detuning of 200 GHz, Fig. 3 center, with the calculation for an ideal situation and without absorption, Fig. 2. The reduction by a factor of about 17 is due to three effects. (1) An imperfect overlap in the fundamental beams and fractional power in the lowest Gaussian beam mode [17] causes an overall reduction in the efficiency by a factor of 4. (2) Absorption in the VUV. The absorption length is 5.1 mm at a VUV detuning of 40 GHz, which has been measured by changing the focus position in the mercury vapor. This corresponds to a reduction of 3 in the VUV yield. (3) Saturation has been observed by changing the fundamental powers and measuring the change in FWM efficiency. (No such saturation was observed in earlier experiments [17,18] because they were at much larger VUV detunings.) Saturation contributes a factor of 1.4. A maximum yield of 6 μW in the VUV was achieved with input powers of 182 mW (UV), 245 mW (blue), 525 mW (green), and detunings of $\Delta_{\mathrm{UV}} = 120$ GHz and $\Delta_{\mathrm{VUV}} = 40$ GHz.

In conclusion, we have demonstrated a high power continuous-wave laser source at 121 nm wavelength. Utilizing the interplay of two resonances at one- and three-photon height, a large increase in FWM efficiency could be achieved. We observed powers up to 6 μW, which is 30 times more than ever achieved in this wavelength region and three orders of magnitude more efficient.

Such a coherent VUV source can be used for direct Rydberg excitation of trapped ions, which is at the heart of a new scheme for fast quantum information processing [4] using the Rydberg blockade [19,20]. An alternate approach for Rydberg excitation is to use several visible lasers in a multistep scheme. In comparison, our VUV laser source is, of course, much more complex. The advantage is, however, that one-step Rydberg excitation of trapped ions has no leaks and is conceptually straightforward.

The authors acknowledge funding through the Bundesministerium für Bildung und Forschung and the ERA-NET CHIST-ERA (R-ION consortium).

*kolbed@uni-mainz.de

†Present address: Carl Zeiss Laser Optics GmbH, Carl Zeiss Strasse, D-73446 Oberkochen, Germany.

[1] G. B. Andresen *et al.*, Nature (London) **468**, 673 (2010).

[2] T. W. Hänsch and C. Zimmermann, Hyperfine Interact. **76**, 47 (1993).

[3] P. Pérez and A. Rosowsky, Nucl. Instrum. Methods Phys. Res., Sect. A **545**, 20 (2005).

[4] M. Müller, L. Liang, I. Lesanovsky, and P. Zoller, New J. Phys. **10**, 093009 (2008).

[5] F. Schmidt-Kaler, T. Feldker, D. Kolbe, J. Walz, M. Müller, P. Zoller, W. Li, and I. Lesanovsky, New J. Phys. **13**, 075014 (2011).

[6] R. Wallenstein, Opt. Commun. **33**, 119 (1980).

[7] J. P. Marangos, N. Shen, H. Ma, M. H. Hutchinson, and J. P. Connerade, J. Opt. Soc. Am. B **7**, 1254 (1990).

[8] C. Vidal, in *Tunable Lasers*, Topics in Applied Physics, edited by L. Mollenauer, J. White, and C. Pollock (Springer-Verlag, Berlin, 1992), Vol. 59, p. 57.

[9] A. V. Smith, W. J. Alford, and G. R. Hadley, J. Opt. Soc. Am. B **5**, 1503 (1988).

[10] K. S. E. Eikema, J. Walz, and T. W. Hänsch, Phys. Rev. Lett. **83**, 3828 (1999).

[11] K. S. E. Eikema, J. Walz, and T. W. Hänsch, Phys. Rev. Lett. **86**, 5679 (2001).

[12] A. Pahl, P. Fendel, B. R. Henrich, J. Walz, T. W. Hänsch, and K. S. E. Eikema, Laser Phys. **15**, 46 (2005).

[13] M. Scheid, F. Markert, J. Walz, J. Wang, M. Kirchner, and T. W. Hänsch, Opt. Lett. **32**, 955 (2007).

[14] F. Markert, M. Scheid, D. Kolbe, and J. Walz, Opt. Express **15**, 14476 (2007).

[15] G. C. Bjorklund, IEEE J. Quantum Electron. **11**, 287 (1975).

[16] A. V. Smith and W. J. Alford, J. Opt. Soc. Am. B **4**, 1765 (1987).

[17] D. Kolbe, A. Beczkowiak, T. Diehl, A. Koglbauer, M. Sattler, M. Stappel, R. Steinborn, and J. Walz, Can. J. Phys. **89**, 25 (2011).

[18] M. Scheid, D. Kolbe, F. Markert, T. W. Hänsch, and J. Walz, Opt. Express **17**, 11274 (2009).

[19] T. Wilk, A. Gaëtan, C. Evellin, J. Wolters, Y. Miroshnychenko, P. Grangier, and A. Browaeys, Phys. Rev. Lett. **104**, 010502 (2010).

[20] L. Isenhower, E. Urban, X. L. Zhang, A. T. Gill, T. Henage, T. A. Johnson, T. G. Walker, and M. Saffman, Phys. Rev. Lett. **104**, 010503 (2010).